Research Square

Preprints are preliminary reports that have not undergone peer review.
They should not be considered conclusive, used to inform clinical practice,
or referenced by the media as validated information.

Spine-Pelvis-Hip Biomechanics of PLIF, TLIF, and LLIF at L4-5: A Finite Element Study in Roussouly Type II Alignment

Yonggui Wu
Tianjin Medical University
Xingze Zhang
Tianjin Medical University
Haochen Hu
Tianjin Medical University
Chao Chen
Tianjin Hospital
Jun Miao
Tianjin Hospital
Qiang Yang
yangqiang1980@126.com

Beijing Friendship Hospital

Research Article

Keywords: Lumbar interbody fusion, Finite element analysis, Roussouly type II alignment, Spine-pelvis-hip chain, Acetabular cartilage

Posted Date: June 10th, 2026

DOI: https://doi.org/10.21203/rs.3.rs-9771694/v1

License: This work is licensed under a Creative Commons Attribution 4.0 International License.
Read Full License

Additional Declarations: No competing interests reported.

Abstract

Background

Lumbar interbody fusion at L4-5 is commonly performed for degenerative lumbar disorders. Patients with Roussouly type II sagittal alignment may have a relatively flat lumbar profile and altered lower-lumbar load transfer, which may influence postoperative adjacent-segment mechanics and implant loading. Most finite element studies of lumbar fusion have focused on the lumbar spine alone, whereas the pelvis and hip joints are rarely included as part of the load-transfer pathway.

Methods

A three-dimensional finite element model of the lumbar spine, pelvis, and bilateral proximal femora was developed from computed tomography data obtained from a healthy adult male volunteer with Roussouly type II alignment. PLIF, TLIF, and LLIF constructs at L4-5 were simulated with bilateral pedicle screw fixation. Under flexion, extension, left and right lateral bending, and left and right axial rotation, von Mises stress distributions were evaluated in the adjacent L3-4 intervertebral disc, the L5 superior endplate, the pedicle screw-rod system, and acetabular cartilage.

Results

All three constructs provided immediate stabilization at the operated segment. Peak stress in the L3-4 nucleus pulposus showed only modest inter-construct differences, whereas stress distribution differed under lateral bending and axial rotation. TLIF produced the highest stress concentration in the posterior fixation system, particularly during lateral bending and axial rotation. Endplate stress was more concentrated in the posterior constructs, while LLIF showed a broader and more homogeneous stress distribution across the L5 superior endplate. Acetabular cartilage stress showed construct-dependent distribution patterns, suggesting altered lumbopelvic load transfer after L4-5 fusion.

Conclusions

In a Roussouly type II finite element model, PLIF, TLIF, and LLIF achieved comparable immediate stabilization at L4-5 but differed in load-sharing behavior. LLIF reduced mechanical demand on posterior instrumentation and produced more homogeneous endplate loading, while TLIF showed greater posterior implant stress concentration. These findings should be interpreted as comparative biomechanical evidence rather than direct proof of clinical superiority.

Introduction

Degenerative disorders of the lower lumbar spine are a common cause of chronic low back pain and functional disability. The L4-5 segment is particularly vulnerable to degeneration because it is exposed to substantial motion and load transfer during daily activity. Previous biomechanical studies have shown that lumbar fusion can alter adjacent-segment mechanics and increase mechanical demand on adjacent discs, facet joints, endplates, and posterior fixation systems [1, 2]. These effects are clinically relevant because postoperative load redistribution is considered one of the mechanical contributors to adjacent segment degeneration and implant-related complications.

Several lumbar interbody fusion techniques have been developed to restore segmental stability and promote interbody fusion. PLIF allows bilateral posterior cage insertion through a posterior midline approach, whereas TLIF uses a unilateral transforaminal corridor and usually places the cage asymmetrically. LLIF accesses the disc space through a lateral corridor and permits placement of a cage with a larger footprint across the apophyseal ring. Although these approaches can all reduce motion at the fused segment, their implant geometry, cage position, and degree of posterior element preservation differ substantially [3, 5]. These anatomic and technical differences provide the mechanical basis for construct-specific load sharing.

Previous finite element and experimental studies have investigated the effects of cage position, cage geometry, posterior complex preservation, and fixation strategies on lumbar fusion biomechanics [3, 5, 9–11, 13–17]. In general, constructs with more effective anterior column support tend to reduce posterior implant loading, whereas asymmetric cage placement or limited anterior support may increase stress in the screw-rod system. Endplate stress is also strongly influenced by cage footprint and contact location, and excessive focal stress may theoretically increase the risk of cage subsidence or endplate injury [9, 10, 24, 25].

Sagittal alignment is another important determinant of lumbar biomechanics. Roussouly type II alignment is characterized by a relatively flat lumbar profile and a low sacral slope, which may reduce sagittal compensatory capacity and predispose the lower lumbar spine to concentrated mechanical loading. However, most finite element models are built from anatomically average spines and do not explicitly incorporate sagittal alignment subtypes. Consequently, the biomechanical consequences of fusion technique selection in a flat-back sagittal profile remain incompletely understood [33, 35].

Another limitation of many existing lumbar finite element studies is that the model often terminates at the sacrum. This approach is useful for evaluating local spinal mechanics, but it neglects the pelvis and hip joints as part of the global load-transfer pathway. The sacroiliac joint and pelvis are important transitional structures between the spine and lower limbs, and prior studies have shown that pelvic mechanics and sacroiliac joint behavior can be influenced by spinal loading and fixation [6, 12, 20, 23, 32]. Moreover, finite element methods have been used to characterize hip cartilage contact stresses, supporting the feasibility of incorporating hip-related structures into integrated biomechanical models [4, 8].

The present study therefore aimed to compare the biomechanical behavior of PLIF, TLIF, and LLIF at L4-5 using a spine-pelvis-hip finite element model based on Roussouly type II alignment. The analysis focused on adjacent disc stress, L5 superior endplate stress, pedicle screw-rod stress, and acetabular cartilage stress. The purpose was not to establish clinical superiority of one surgical approach over another, but to characterize construct-dependent load-sharing patterns within an integrated lumbopelvic biomechanical framework.

Materials and methods

Finite element model construction

A three-dimensional finite element (FE) model of the lumbar spine (L1-S1), pelvis, and bilateral proximal femora was developed from computed tomography (CT) data obtained from a healthy adult male volunteer (26 years old; body weight, 67 kg). The subject had no history of spinal, pelvic, or hip disease and showed no radiographic evidence of structural spinal or hip pathology. Written informed consent was obtained, and the study protocol was approved by the institutional review board of the authors' institution.

A healthy young subject was selected to establish a geometrically controlled baseline model and to minimize confounding effects caused by advanced degeneration, osteophyte formation, collapse, deformity, or asymmetric joint degeneration. This choice was intended to support controlled comparison among the three fusion constructs rather than to reproduce all features of the older degenerative population typically undergoing lumbar fusion.

CT images were acquired using a 64-slice spiral CT scanner (Siemens, Erlangen, Germany) with a slice thickness of 0.625 mm. The imaging dataset included the lumbar vertebrae, sacrum, bilateral pelvic bones, and proximal femora. DICOM data were imported into Mimics 21.0 (Materialise Inc., Leuven, Belgium) for segmentation and surface reconstruction. Three-dimensional surface models were exported as STL files and further refined in 3-matic 13.0 (Materialise Inc.) and Geomagic Studio 2021 (Geomagic Inc., USA). Excessive smoothing was avoided to preserve anatomic fidelity. Intervertebral discs, nucleus pulposus, annulus fibrosus, facet joints, posterior elements, pedicle screws, rods, and cages were constructed in SolidWorks 2025 SP0 (Dassault Systemes, USA). All components were assembled and meshed in HyperMesh 2022 (Altair Engineering, Troy, MI, USA), and the final analyses were performed in Abaqus 2022 (Dassault Systemes, USA).

Material properties were assigned according to published FE studies and are summarized in Table 1 [4–8, 12, 18, 24, 25]. Cortical bone thickness was set to 1 mm and cartilaginous endplate thickness to 0.5 mm. The nucleus pulposus accounted for approximately 43–44% of total disc volume. The annulus fibrosus was modeled as five concentric layers of annulus ground substance reinforced by collagen fibers, with fiber orientation ranging from 25 degrees to 45 degrees relative to the horizontal plane. The elastic modulus of annulus fibers increased from 360 MPa in the innermost layer to 550 MPa in the

outermost layer. Facet joint contacts were defined as frictionless, whereas the pubic symphysis was defined as rough contact. To reduce computational complexity and permit controlled comparison, acetabular cartilage was bonded to the femoral head and acetabulum.

Table 1
Material properties defined in the FE model

Component	Young's modulus (MPa)	Poisson's ratio	Cross-sectional area (mm^2)
Bony structures			
Lumbar cortical bone	12000	0.3	-
Lumbar cancellous bone	100	0.2	-
Lumbar posterior element	3500	0.25	-
Sacral and iliac cortical bone	17000	0.3	-
Sacral and iliac cancellous bone	100	0.2	-
Femur cortical bone	17000	0.3	-
Femur cancellous bone	17000	0.2	-
Facet joint cartilage	11	0.2	-
Sacroiliac articular cartilage	29	0.49	-
Pubic symphysis	5	0.45	-
Acetabular cartilage	100	0.3	-
Intervertebral disc			
Annulus fibres	360–550	-	0.15
Matrix	2	0.45	-
Nucleus pulpous	1	0.49	-
Cartilaginous endplate	24	0.4	-
Ligaments			
ALL	7.8	-	63.7
PLL	10	-	20
LF	15	-	40
ISL	10	-	40
SSL	8	-	30
CL	7.5	-	30
ITL	10	-	1.8
Implants			

Component	Young's modulus (MPa)	Poisson's ratio	Cross-sectional area (mm^2)
Cage (titanium alloy)	110,000	0.3	
Bone graft	100	0.2	
Screws and rods (titanium alloy)	110,000	0.3	

Surgical simulation

For all surgical models, the L4-5 intervertebral disc was completely removed and interbody fusion cages were implanted into the disc space. The cages were filled with cancellous bone to simulate packed bone graft material. The grafting region within the intervertebral space was defined according to previous finite element studies of lumbar interbody fusion [14, 18, 19].

In the PLIF model, partial laminectomy and medial facetectomy were simulated. The supraspinous ligament, interspinous ligament, ligamentum flavum, and posterior longitudinal ligament were removed, and two posterior cages (22 mm x 10 mm x 10 mm; lordotic angle, 0 degrees) were inserted bilaterally. In the TLIF model, the left facet joint, ligamentum flavum, and posterior longitudinal ligament were resected, and one cage (22 mm x 10 mm x 10 mm; lordotic angle, 0 degrees) was inserted through a unilateral transforaminal corridor. In the LLIF model, a lateral cage (50 mm x 20 mm x 12 mm; lordotic angle, 8 degrees) was placed across the L4-5 disc space to represent a typical lateral cage footprint [16, 17].

All fusion models were supplemented with bilateral pedicle screw fixation, consisting of four pedicle screws (6 mm in diameter and 45 mm in length) and two longitudinal rods (6 mm in diameter). To avoid artificial mesh-related stress peaks, cage serrations and pedicle screw threads were not modeled, consistent with common comparative finite element practice [16, 24]. Implant-bone and implant-graft interfaces were defined as bonded contacts. This idealized setting allowed standardized comparison among constructs but represented an immediate postoperative mechanical condition rather than biological osseointegration.

Model validation

Model validation was performed by comparing predicted range of motion (ROM) values with previously published cadaveric and computational data [12, 18, 21, 22]. For validation of the L1-S1 lumbar model, the inferior surface of the sacrum was fixed, and pure moments were applied to the superior surface of L1: 8 N-m in flexion, 6 N-m in extension, +/-6 N-m in lateral bending, and +/-4 N-m in axial rotation. For sacroiliac joint validation, the right femur was fixed and a 7.5 N-m pure moment was applied to the

superior surface of L4. Flexion-extension, lateral bending, and axial rotation were defined as sagittal, coronal, and transverse plane motions, respectively.

The validation analysis was used to confirm that the intact model produced physiologically reasonable motion behavior before surgical simulation. The primary aim of validation was to support relative comparison among PLIF, TLIF, and LLIF constructs rather than to reproduce patient-specific clinical motion in vivo.

Boundary and loading conditions

For surgical simulations, both femora were fixed in all directions to constrain pelvic motion and permit standardized comparison of load transfer across constructs. A compressive follower load of 500 N was applied to the superior surface of L1 to simulate upper body load, and a pure moment of 7.5 N-m was applied to generate six loading conditions: flexion (FL), extension (EX), left lateral bending (LLB), right lateral bending (RLB), left axial rotation (LAR), and right axial rotation (RAR) [18, 35].

The loading protocol was selected to compare construct-dependent biomechanical responses under identical boundary conditions rather than to reproduce a specific clinical activity. Peak von Mises stress values and stress distribution patterns were recorded for the adjacent L3-4 intervertebral disc, the L5 superior endplate, pedicle screws, rods, and acetabular cartilage.

Results

Validation of the finite element model

The intact finite element model demonstrated acceptable agreement with previously published experimental and computational ROM data [12, 18, 21, 22]. Segmental motion patterns under flexion-extension, lateral bending, and axial rotation were consistent with reported physiological trends. The validated model was therefore considered suitable for comparative biomechanical analysis of the three L4-5 fusion constructs.

Finite element models of the three fusion constructs

The PLIF, TLIF, and LLIF models are shown in Fig. 1. The posterior constructs differed mainly in cage number and placement, with PLIF using bilateral posterior cages and TLIF using a unilateral oblique cage. LLIF was characterized by a larger laterally inserted cage footprint with broader endplate coverage. All constructs included bilateral pedicle screw fixation, allowing differences in stress behavior to be attributed primarily to cage configuration, anterior column support, and preservation or resection of posterior elements.

Adjacent segment disc mechanics

Peak von Mises stress in the L3-4 nucleus pulposus showed only modest differences among PLIF, TLIF, and LLIF (Fig. 2). Extension produced the highest nucleus stress across all constructs. Under lateral bending and axial rotation, stress distribution patterns differed more clearly than peak values. LLIF maintained a relatively homogeneous stress pattern, whereas posterior constructs showed more localized stress concentration in certain loading directions. These findings suggest that the influence of fusion strategy on the adjacent disc was more evident in stress distribution than in absolute peak nucleus stress.

Stress distribution at the fused segment endplate

The superior endplate of L5 showed construct-dependent stress behavior (Fig. 4). During flexion, lateral bending, and axial rotation, TLIF generated the most pronounced focal stress concentration. PLIF showed an intermediate pattern, whereas LLIF demonstrated broader load distribution across the endplate. In all constructs, high-stress regions were mainly located in the posterior portion of the L5 superior endplate, but the degree of localization varied substantially among techniques.

Pedicle screw and rod stress

Stress within the posterior fixation system differed markedly among constructs (Figs. 3 and 4). TLIF consistently generated the highest pedicle screw and rod stresses, particularly during lateral bending and axial rotation. PLIF showed lower stress than TLIF but higher stress than LLIF under most loading conditions. LLIF demonstrated the lowest overall posterior instrumentation stress, indicating reduced mechanical demand on the screw-rod system.

Overall stress behavior of the screw-rod system

Stress contour maps showed that peak stress was generally concentrated near the rod-screw junctions. The TLIF construct demonstrated more pronounced and localized stress accumulation, whereas LLIF showed a more homogeneous stress distribution along the fixation system. These findings indicate that asymmetric posterior cage placement may increase posterior fixation loading, while a larger lateral cage may improve anterior load sharing and reduce posterior implant stress.

Acetabular cartilage stress

Acetabular cartilage stress analysis showed that peak stress regions were generally located in the superior load-bearing portion of the acetabulum (Fig. 5). Although overall peak stress magnitude was comparable among constructs, the spatial distribution and symmetry of acetabular stress differed across loading directions. These construct-dependent patterns suggest that L4-5 fusion strategy may influence downstream load transmission through the pelvis and hip joint, although the findings should be interpreted cautiously because of the simplified hip contact assumptions.

Discussion

This finite element study compared PLIF, TLIF, and LLIF at L4-5 in an integrated spine-pelvis-hip model based on Roussouly type II alignment. The principal finding was that the three constructs achieved comparable immediate stabilization but differed substantially in load-sharing behavior. TLIF produced greater posterior implant stress and more localized endplate loading, whereas LLIF demonstrated lower posterior instrumentation stress and broader endplate load distribution. These findings are consistent with previous reports indicating that cage position, cage footprint, and anterior column support strongly influence implant stress and endplate mechanics after lumbar interbody fusion [10, 14–16, 24, 25].

The adjacent segment findings require cautious interpretation. Peak stress in the L3-4 nucleus pulposus was broadly similar among constructs, suggesting that all three fusion strategies imposed comparable immediate adjacent-level nuclear stress under the present boundary conditions. However, stress distribution patterns differed under lateral bending and axial rotation. Prior finite element studies have shown that posterior complex disruption and rigid segmental fixation may influence adjacent segment stress and motion [1, 3, 5, 21, 22]. In the present model, LLIF appeared to preserve a more uniform adjacent disc stress pattern, probably because broader anterior support reduced focal load transfer during asymmetric loading.

The higher posterior implant stress observed in TLIF can be explained mechanically by unilateral cage placement and reduced symmetric anterior column support. When anterior support is eccentric, a larger proportion of bending and rotational load may be transferred through the posterior screw-rod system. This is consistent with previous comparative studies showing that lateral or anteriorly supported constructs may reduce posterior instrumentation stress, whereas asymmetric or less supportive cage configurations increase implant loading [13–17, 26, 28]. From a biomechanical perspective, such stress concentration may be relevant because repetitive posterior implant loading can contribute to screw loosening, rod fatigue, or construct failure in susceptible patients, although finite element stress alone cannot establish clinical failure risk [19, 22].

Endplate stress distribution is another clinically relevant biomechanical outcome. TLIF generated the most localized L5 superior endplate stress, whereas LLIF showed broader stress distribution. This difference is likely related to cage footprint. Larger cages that span a wider portion of the apophyseal ring can distribute load over a greater contact area, thereby reducing focal endplate stress. This concept is supported by previous studies examining cage position, cage geometry, and ring apophysis support in lumbar interbody fusion [9, 10, 24, 25, 31]. In contrast, smaller posterior cages may create localized posterior endplate stress, especially during bending and rotation.

The inclusion of acetabular cartilage stress is an important feature of the present study. Lumbar fusion is not an isolated spinal event; it may alter load transfer across the sacrum, pelvis, sacroiliac joints, and hip joints. Previous studies have emphasized the role of pelvic and sacroiliac biomechanics in spinal load transmission [6, 12, 20, 23, 32]. In the present model, acetabular peak stress magnitude was broadly comparable among constructs, but stress symmetry and spatial distribution differed under several

loading conditions. These findings suggest that different L4-5 fusion strategies may subtly alter the spine-pelvis-hip load-transfer pathway. However, the acetabular cartilage results should be viewed as exploratory biomechanical context rather than direct evidence of hip joint degeneration or clinical hip symptoms [4, 7, 8].

The present findings may be particularly relevant to patients with Roussouly type II alignment. A flatter sagittal profile may reduce the capacity for physiologic lumbar compensation and may increase mechanical demand at the lower lumbar segments. Although the present model was derived from a single young volunteer and cannot represent the full anatomic variability of all Roussouly type II patients, it provides an alignment-specific framework for comparing fusion strategies. Previous work has demonstrated that sagittal alignment can influence lumbar biomechanics and that different fixation strategies may behave differently under distinct sagittal profiles [33, 35].

Several limitations must be acknowledged. First, the model was based on a single healthy young male volunteer rather than an older patient with degenerative lumbar disease. The model therefore does not incorporate disc degeneration, facet arthrosis, osteophytes, osteoporosis, or patient-specific degenerative deformity. Second, muscle forces were not explicitly simulated, and a simplified follower load was used. Third, implant-bone interfaces were assumed to be bonded, which standardizes comparison but does not reproduce immediate postoperative micromotion. Fourth, the LLIF cage had an 8-degree lordotic angle, whereas the PLIF and TLIF cages had 0-degree lordosis. Therefore, differences between constructs may reflect both surgical approach and cage geometry. Fifth, both femora were fixed and acetabular cartilage was bonded, which limits direct interpretation of hip cartilage stress. Finally, mesh convergence and sensitivity analyses should be further reported in future work to improve numerical robustness.

Despite these limitations, the use of an identical modeling framework for all three constructs permits meaningful relative comparison. The results suggest that fusion technique selection may influence not only local segmental mechanics but also broader lumbopelvic load transfer. For BMC Musculoskeletal Disorders, the clinical value of these findings lies not in claiming superiority of LLIF, but in clarifying how construct geometry and alignment-specific mechanics interact in the spine-pelvis-hip chain.

Conclusions

In a Roussouly type II finite element model, PLIF, TLIF, and LLIF achieved comparable immediate stabilization at L4-5 but demonstrated distinct load-sharing characteristics. TLIF was associated with greater stress concentration in the posterior fixation system and at the L5 superior endplate, whereas LLIF showed broader endplate load distribution and reduced posterior instrumentation stress. Acetabular cartilage stress patterns also differed among constructs, suggesting construct-dependent alterations in lumbopelvic load transfer. These findings provide comparative biomechanical evidence to support surgical planning in patients with flat-back sagittal alignment, but they should be interpreted cautiously because of the inherent limitations of single-subject finite element modeling.

Abbreviations

ALL: anterior longitudinal ligament; BPSF: bilateral pedicle screw fixation; CL: capsular ligament; CT: computed tomography; EX: extension; FE: finite element; FL: flexion; ISL: interspinous ligament; ITL: intertransverse ligament; LAR: left axial rotation; LF: ligamentum flavum; LLB: left lateral bending; LLIF: lateral lumbar interbody fusion; PLIF: posterior lumbar interbody fusion; PLL: posterior longitudinal ligament; RAR: right axial rotation; RLB: right lateral bending; ROM: range of motion; SSL: supraspinous ligament; TLIF: transforaminal lumbar interbody fusion.

Declarations

Ethics approval and consent to participate: The study protocol was approved by the Institutional Review Board of the authors' institution. Written informed consent was obtained from the volunteer. This study was approved by the ethics committee of Tianjin Hospital (Registration number: 2025-056) and the research was performed in accordance with the guidelines of the Declaration of Helsinki. Informed consent for this study was obtained from all patients by both written and verbal.

Consent for publication: Not applicable.

Availability of data and materials: The datasets used and analyzed during the current study are available from the corresponding author on reasonable request.

Competing interests: The authors declare that they have no competing interests.

Funding: This research received no specific grant from any funding agency in the public, commercial, or not-for-profit sectors.

Authors' contributions: YW, XZ, and HH contributed to model construction, data analysis, and manuscript drafting. QY, JM, and CC contributed to study conception, supervision, interpretation of results, and critical revision of the manuscript. All authors read and approved the final manuscript.

Acknowledgements: The authors thank all colleagues who provided technical support and valuable discussions during finite element model development and manuscript preparation.

References

1. Chen Y, Wang H, Sun J, Liu H. Biomechanical effects of lumbar fusion on adjacent segments. J Biomech. 2018;76:199–206.
2. Chen Z, Sun J, Wang H, Liu Y. Biomechanical evaluation of lumbar fusion techniques using finite element modeling. Eur Spine J. 2018;27(6):1356–64.

3. Fan W, Guo LX, Zhao D. Posterior lumbar interbody fusion versus transforaminal lumbar interbody fusion: finite element analysis of the vibration characteristics of fused lumbar spine. World Neurosurg. 2021;150:e81–8.
4. Harris MD, Anderson AE, Henak CR, Ellis BJ, Peters CL, Weiss JA. Finite element prediction of cartilage contact stresses in normal human hips. J Orthop Res. 2012;30:1133–9.
5. Huang YP, Du CF, Cheng CK, et al. Preserving posterior complex can prevent adjacent segment disease following posterior lumbar interbody fusion surgeries: a finite element analysis. PLoS ONE. 2016;11:e0166452.
6. Joukar A, Shah A, Kiapour A, et al. Sex-specific sacroiliac joint biomechanics during standing upright: a finite element study. Spine. 2018;43:E1053–60.
7. Kang S, Chang MC, Kim H, et al. The effects of paraspinal muscle volume on physiological load on the lumbar vertebral column: a finite-element study. Spine. 2021;46:E1015–21.
8. Kwak DK, Lee Y, Lee SJ, Lee S, Yoo JH. What is the appropriate axial position in cannulated screw fixation for femoral neck fractures? A finite element analysis. BMC Musculoskelet Disord. 2025;26:430.
9. Li H, Liu J, Cui H, et al. The effects of cage on endplate collapse after stand-alone OLIF: based on finite element analysis and in vitro mechanics experiments. Front Bioeng Biotechnol. 2024;12:1508385.
10. Li X, Zhang Y, Wang Q, Chen J, Zhou Y, et al. Effects of cage position on stress distribution after lumbar interbody fusion: a finite element study. Clin Biomech Elsevier Ltd. 2021;84:105326.
11. Li Y, Zhao X, Zhang Q, Wang D, et al. Three-dimensional finite element study of lumbar spine stability after fusion. Clin Biomech Elsevier Ltd. 2021;83:105292.
12. Lindsey DP, Perez-Orribo L, Rodriguez-Martinez N, et al. Evaluation of a minimally invasive procedure for sacroiliac joint fusion: an in vitro biomechanical analysis of initial and cycled properties. Med Devices: Evid Res. 2014;7:131–7.
13. Liu H, Chen W, Xu Z, Zhang J. Biomechanical comparison of different fixation strategies in lumbar fusion. J Orthop Res. 2019;37(9):1985–93.
14. Lu T, Ren J, Sun Z, et al. Relationship between the elastic modulus of the cage material and the biomechanical properties of transforaminal lumbar interbody fusion: a logarithmic regression analysis based on parametric finite element simulations. Comput Methods Programs Biomed. 2022;214:106570.
15. Lu T, Sun Z, Xia H, et al. Comparing the osteogenesis outcomes of different lumbar interbody fusions (ALIF/OLIF/XLIF/TLIF/PLIF) by evaluating their mechano-driven fusion processes. Comput Biol Med. 2024;171:108215.
16. Oikawa R, Murakami H, Endo H, et al. Comparison of the susceptibility to implant failure in the lateral, posterior, and transforaminal lumbar interbody fusion: a finite element analysis. World Neurosurg. 2022;164:e835–43.

17. Pradeep K, Pal B, Mukherjee K, Shetty GM. Transforaminal lumbar interbody fusion surgery: a finite element analysis of open and minimally invasive approaches at the L4-L5 segment. Heliyon. 2025;11:e02222.
18. Renner SM, Natarajan RN, Patwardhan AG, et al. Novel model to analyze the effect of a large compressive follower pre-load on range of motions in a lumbar spine. J Biomech. 2007;40:1326–32.
19. Shin JK, Lim BY, Goh TS, et al. Effect of the screw type, screw length, and screw head angle on the risk of screw and adjacent bone failures after spinopelvic fixation: a finite element analysis. PLoS ONE. 2018;13:e0201801.
20. Sun Y, Fu Y, Liu F, et al. Biomechanical tests and finite element analyses of pelvic stability using bilateral single iliac screws with different channels in lumbo-iliac fixation. Front Surg. 2022;9:1035614.
21. Sun Y, Zhang K, Li R, Wang P, Zhao J, et al. Finite element analysis of adjacent segment biomechanics following lumbar fusion. Clin Biomech Elsevier Ltd. 2020;72:102–9.
22. Tan Q, Liu Z, Zhao Y, et al. Biomechanical comparison of four types of instrumentation constructs for revision surgery in lumbar adjacent segment disease: a finite element study. Comput Biol Med. 2021;134:104477.
23. Wang D, Shi D, Li X, Wang F. Three-dimensional finite element analysis of load transmission in the human pelvis. Med Eng Phys. 2018;60:1–8.
24. Wang J, Geng Z, Ma X, Zhang Z, Miao J. Comparative analysis of cages crossing the vertebral ring apophysis in normal and osteoporotic models under endplate injury: a finite element analysis. Front Bioeng Biotechnol. 2023;11:1263751.
25. Wang J, Geng Z, Wu J, et al. Biomechanical properties of lumbar vertebral ring apophysis cages under endplate injury: a finite element analysis. BMC Musculoskelet Disord. 2023;24:695.
26. Wang Q, Li X, Shi D, Zhang Y. Biomechanical comparison of lumbar fixation techniques using finite element analysis. Eur Spine J. 2020;29(4):892–900.
27. Wang X, Liu W, Zhao Y, Ma P. The impact of disc degeneration on the dynamic characteristics of the lumbar spine: a finite element analysis. Front Bioeng Biotechnol. 2024;12:1384187.
28. Wu J, Yang D, Han Y, et al. Application of dual-trajectory screws in revision surgery for lumbar adjacent segment disease: a finite element study. J Orthop Surg Res. 2022;17:1–11.
29. Xu H, Wen W, Yang D, Han Y. Biomechanical analysis of lumbar degeneration based on finite element modeling. Clin Biomech Elsevier Ltd. 2018;58:1–7.
30. Yang D, Han Y, Xu H, Wen W, Xu H. Application of finite element analysis in orthopedic biomechanics. Clin Biomech Elsevier Ltd. 2019;63:14–22.
31. Zhang T, Liu Z, Wang Y, Li J. Finite element evaluation of different interbody fusion cages in the lumbar spine. Spine J. 2019;19(6):1040–8.
32. Zhang W, Cheng Y, Diarra MD, et al. Finite element analysis of sacral-alar-iliac screw fixation for sacroiliac joint dislocation. J Orthop Res. 2023;41:1821–30.

33. Zhou Y, Li C, Wang L, Chen H. Influence of sagittal alignment on lumbar spine biomechanics: a finite element study. Eur Spine J. 2017;26(8):2036–44.
34. Zhu H, Zhong W, Zhang P, et al. Biomechanical evaluation of autologous bone-cage in posterior lumbar interbody fusion: a finite element analysis. BMC Musculoskelet Disord. 2020;21:379.
35. Wang W, Kong C, Pan F, Wu X, Pei B, Lu S. Effects of dynamic and rigid implantation on biomechanical characteristics of different sagittal alignment lumbar after single- or double-level spinal fixations: a finite-element modeling study. Eur J Med Res. 2023;28(1):583. 10.1186/s40001-023-01475-y.

Figures

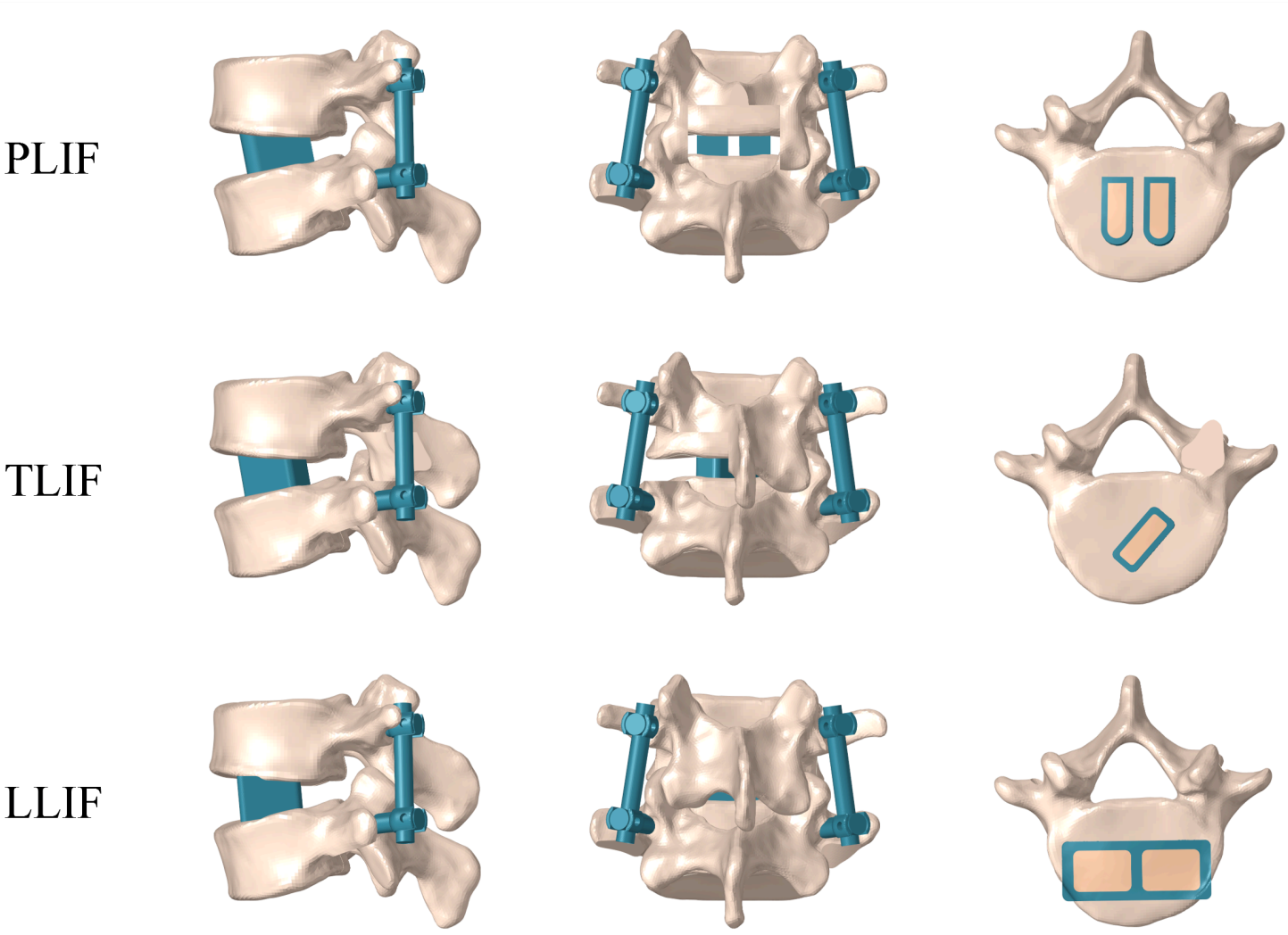


Figure 1

Finite element models of the three L4-5 fusion constructs. PLIF, TLIF, and LLIF were simulated with bilateral pedicle screw fixation. Lateral, posterior, and axial views demonstrate the different cage positions and cage footprints among the three constructs.

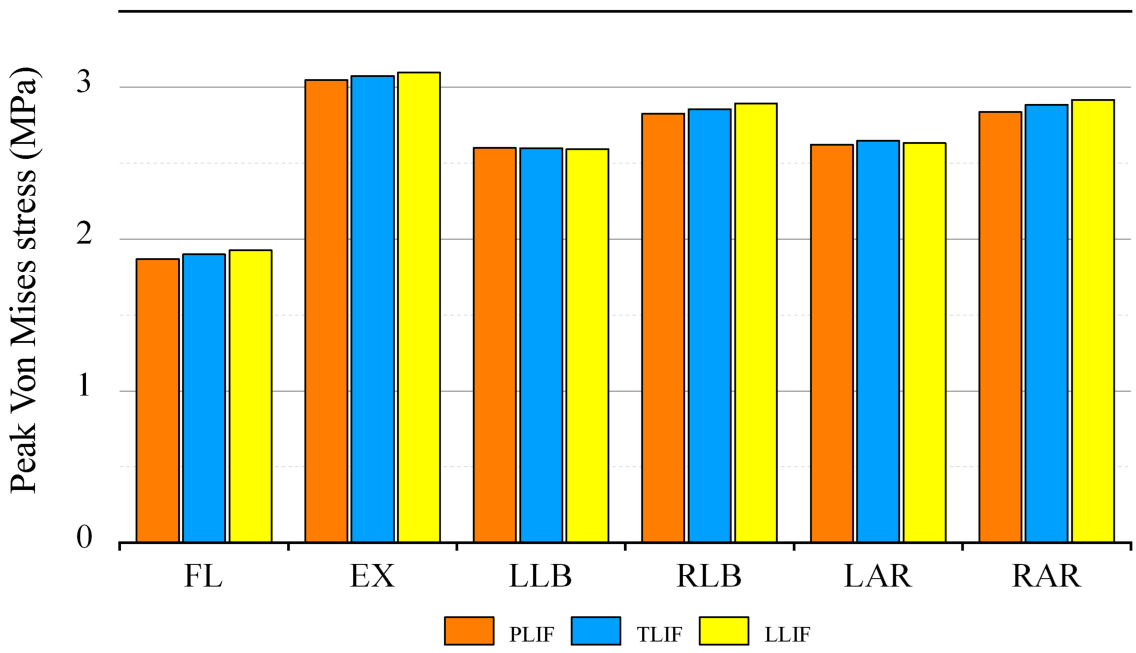


Figure 2

Peak von Mises stress of the L3-4 intervertebral disc nucleus under six loading conditions. FL flexion, EX extension, LLB left lateral bending, RLB right lateral bending, LAR left axial rotation, RAR right axial rotation.

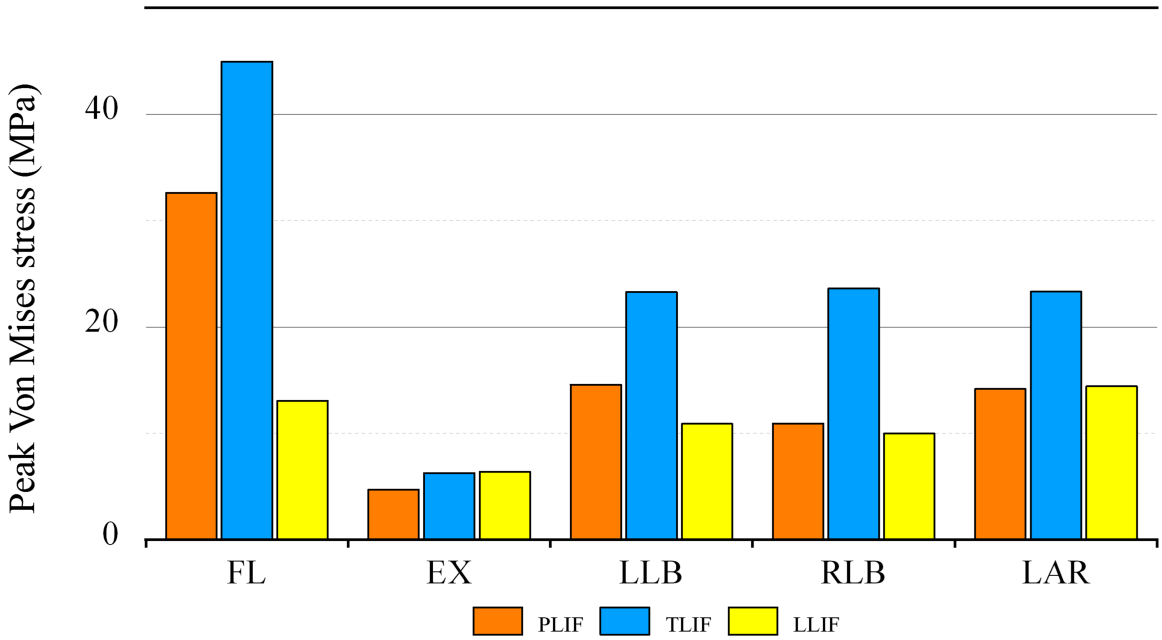


Figure 3

Peak von Mises stress of the pedicle screw-rod system under six loading conditions. TLIF showed higher posterior instrumentation stress than PLIF and LLIF, particularly during lateral bending and axial rotation.

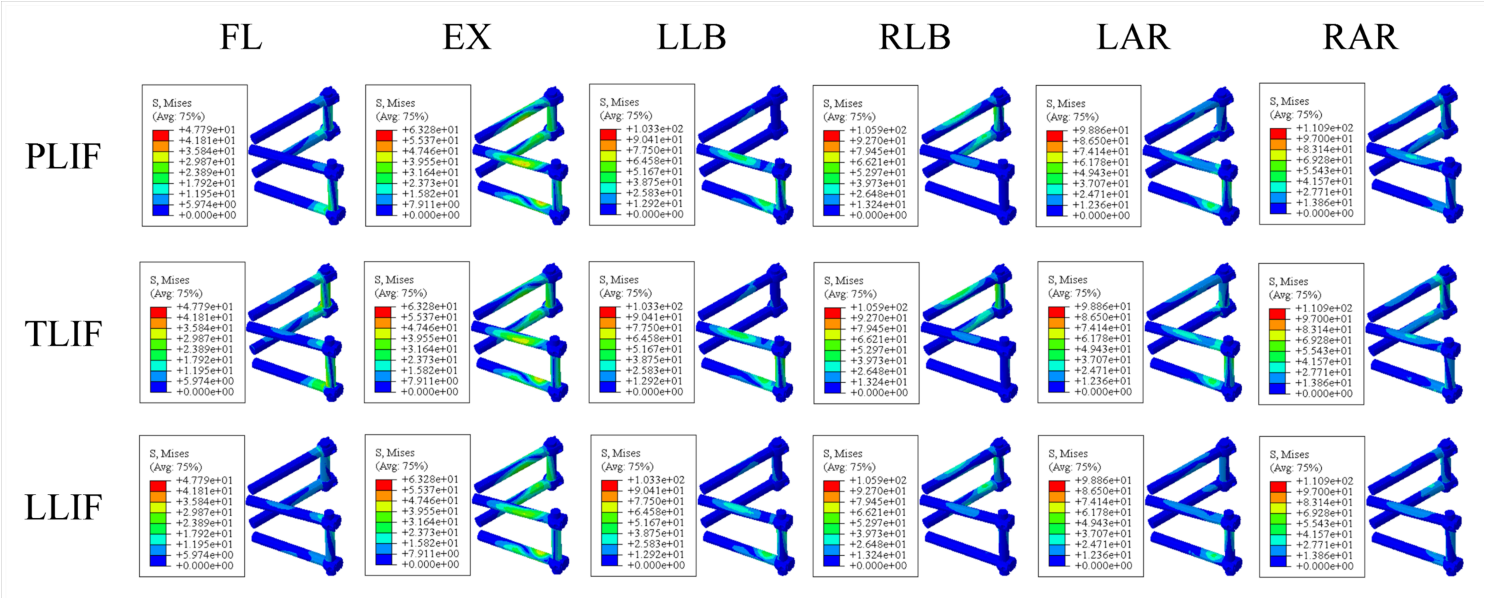


Figure 4

Peak von Mises stress of the L5 superior endplate under six loading conditions. Posterior constructs showed more localized stress concentration, whereas LLIF demonstrated broader endplate load distribution.

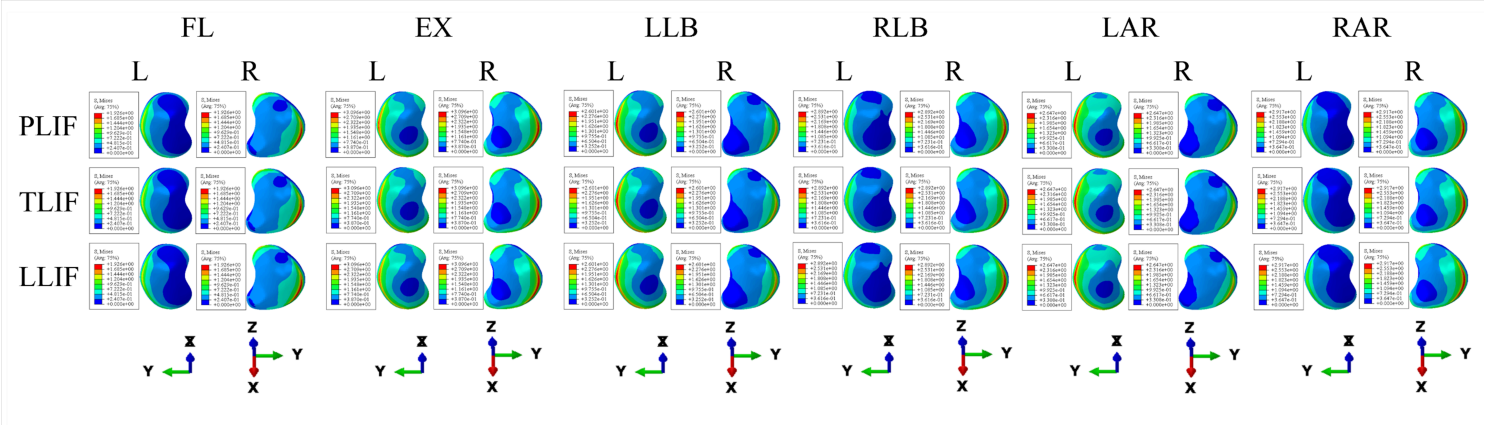


Figure 5

Acetabular cartilage stress distribution in PLIF, TLIF, and LLIF constructs under flexion, extension, lateral bending, and axial rotation. L and R indicate left and right acetabular cartilage, respectively.

Supplementary Files

This is a list of supplementary files associated with this preprint. Click to download.

- model.tif
- Endplatestress.tif